

Article

Photonic Crystal-Supported Long-Range Surface Plasmon-Polaritons Propagating Along High-Quality Silver Nanofilms

Sergey K. Sekatskii ^{1,*}, Anton Smirnov ¹, Giovanni Dietler ¹, Mohammad Nur E. Alam ², Mikhail Vasiliev ² and Kamal Alameh ²

¹ Laboratoire de Physique de la Matière Vivante, IPHYS, Ecole Polytechnique Fédérale de Lausanne, BSP, CH 1015 Lausanne, Switzerland; anton.smirnov@epfl.ch (A.S.); giovanni.dietler@epfl.ch (G.D.)

² Electron Science Research Institute, Edith Cowan University, 270 Joondalup Dr., Joondalup WA 6027, Australia; m.nur-e-alam@ecu.edu.au (M.N.E.A.); m.vasiliev@ecu.edu.au (M.V.); k.alameh@ecu.edu.au (K.A.)

* Correspondence: sergei.sekatski@epfl.ch; Tel.: +41-21-693-0445

Received: 22 November 2017; Accepted: 2 February 2018; Published: 6 February 2018

Abstract: Long-range surface plasmon-polaritons (LRSP) with a propagation length equal to 180 microns at the wavelength of 633 nm have been observed at the interface of 12.5 nm-thick silver nanofilm, coated by a 20 nm-thick protective ZnS layer, with air. Their propagation has been supported by a specially prepared 40-layer 1D Photonic Crystal designed in such a manner that silver layer has been deposited directly onto thin ZnS layer, earlier shown to be a non-oxide material most suitable for the preparation of high-quality thin silver nanofilms.

Keywords: long range surface plasmon polariton; silver nanofilm; 1D photon crystal

1. Introduction

This is well known that thin (no thicker than a few tens of nanometers) metal layers sandwiched between two dielectrics having the same refraction indices (RI) support the propagation of long-range surface plasmon polaritons (LRSP) appearing as a result of the interference of SPP pertinent to the two neighboring metal-dielectric interfaces [1–3]. (For brevity, below we will usually omit the word polariton speaking simply about surface plasmons). Besides fundamental researches, during previous years this effect has been used also for sensing purposes, somewhat analogously (but with certain advantages caused by the long propagation distances in the case) to more standard surface plasmon resonance (SPR)-based sensors (see e.g., [4,5] for general reviews of the field). Both (almost) free-standing thin metal layers, and such layers working in water and deposited onto an appropriate substratum made from material having the same RI as the water (e.g., particular Teflon) were exploited [6,7]. However, certainly, the necessity to construct a symmetric “sandwich” structure to support the LRSP propagation poses a serious problem to be overcome and limits further development of the method. This is true even when the exploitation of such an approach in water is at stake (water’s relatively low refraction index $n = 1.33$ drastically limits the choice of appropriate supports) and makes the work almost impossible in gases as their RI is very close to unity.

The situation has changed completely when it was recognized that somewhat similar situation occurs when one of the dielectrics of a symmetrical sandwich structure is replaced with a specially designed Photonic Crystal (PC) [8]. This enabled the launch and use of surface plasmons (in the red spectral region) for such “non-plasmonic” materials as palladium [9–11] and cobalt [12], as well as launch and use blue (at 405 nm [13]) surface plasmons for gold. Note, that in all of the above cases, without the properly designed Photonic Crystal supporting LRSP, there is simply no point in

speaking about surface plasmons at all: their propagation distances would then be just of the order of the wavelength.

Another big topic is the use of PC-supported surface electromagnetic waves without any metal layer, which has numerous implications in sensorics, electromagnetic field control at the surface and so forth. This topic is relatively far from the research under discussion now, but for completeness, we still would like to indicate a few corresponding essential papers and reviews [14–22], see further references therein.

In this paper, we report on the realization of PC-supported long-range surface plasmons for silver at the red wavelength of He-Ne laser, $\lambda = 632.8$ nm. Quite narrow plasmon resonances, attesting to the ultralong SPP propagation and high quality of silver films, were observed. From one point of view, silver is always considered as the best surface plasmon-supporting metal in the red and near-infrared spectral ranges. However, from another point of view, the difficulties in the preparation of high-quality thin layers of silver and rapid degradation of this material exposed to the atmosphere make its exploitation quite tricky. To the best of our knowledge, up to date LRSP with thin silver nanofilms have been realized only with the (almost) symmetrical sandwich structures composed of silica and (very) thick layers of an index matching oil or polymer [23,24], so that their exploitation as sensors seems not possible.

We also profit a lot from the extensive experience of preparation of thin silver layers onto different dielectrics gained by the Australian team, especially in the course of the researches aiming at the optimization of thin film coatings for solar and thermal radiation control, see e.g., [25,26]. Important peculiarity here is the use of materials, which are not oxide materials, as adjacent layers for silver. Detailed discussion of this point is given in the next Section.

2. Photon Crystal Design

The following structure (see Figure 1) has been designed and prepared to realize LRSP propagation along silver-ZnS/air interface: $\text{SiO}_2/(\text{HL})^{19}/\text{Al}_2\text{O}_3/\text{ZnS}(1)/\text{Ag}/\text{ZnS}(2)/\text{air}$, where SiO_2 are standard 2.3 mm thick fused silica plate, $(\text{HL})^{19}$ are 19 pairs of tantalum pentoxide and silicon dioxide layers (that is transparent dielectrics having high and low refraction indices which form a 1D Photonic Crystal) with the thicknesses respectively 96.6 and 134.4 nm, Al_2O_3 layer has a thickness of 20 nm, ZnS layers 1 and 2 have the thicknesses respectively 52 and 20 nm, Ag is 12.5 nm-thick silver layer. $\text{SiO}_2/(\text{HL})^{19}$ Photonic Crystal on silica substrate has been prepared by magnetron sputtering in one coating run, and afterward all other layers have been deposited on top of this finished structure also in one (but another) coating run.

In the Introduction, we already mentioned the usefulness of the exploitation of non-oxide materials together with metal nanofilms [25,26]. (Shortcomings related with the use of broadly accepted oxide materials for such purposes, e.g., an easy oxidation of ultrathin metal layers, strong tendency of such layers to form nanoparticle islands or agglomerates in the absence of any special “wetting layers” or the like, are discussed in the same references and elsewhere). Through extensive experimentation with ultrathin (sub-15 nm) Ag layers deposited by either thermal evaporation or sputtering, we have found that one possible solution to improve the thin layer morphology (preventing island-type growth) was to carefully select the underlying layer chemistry, and established that ZnS sublayers (substrate layers for Ag) led consistently to improving the layer morphology. In particular, the near IR reflection/transmission (R/T) spectra of custom-designed low-emissivity multilayer coatings employing them have been systematically studied. It is well-known that when the morphology of layers is compromised (island growth with holes in-between takes place), this unavoidably leads to the insufficient reflection of near-IR light by these layers and the coatings based on them. Only if the R/T spectra of multilayer coatings employing at least two Ag layers of thickness below 15 nm are fitted very closely with the spectra predicted using the data pertinent for idealized Ag layers (bulk n and k data), we could conclude that the morphology of growth is close to an ideal one. Exactly such a situation takes place in practice, which allows us to claim the quality of ultrathin silver layers when

ZnS substrate layer was used. A thickness of 12.5 nm for the silver layer has been selected as the minimal thickness for which, according to our experience, high-quality of the film is achieved.

For the principles of optimal PC design see [27]. The thicknesses of H and L layers forming PC were selected following the procedure optimizing the extinction per unit length (for a given wavelength and external media, of course), the thickness of the ZnS(2) layer of $d_{\text{ZnS}2} = 20$ nm was selected as “the smallest sufficient” to protect the silver layer from atmosphere. Al_2O_3 layer (of again the smallest reasonable thickness) was used to improve the quality and adhesion of the first ZnS(1) layer. Finally, we optimize the thickness of this same first internal ZnS(1) layer to achieve the most favorable conditions for LRSPP propagation, and optimize the number of pairs of layers in PC to have the maximal amplification of the light wave on the silver-ZnS interface.

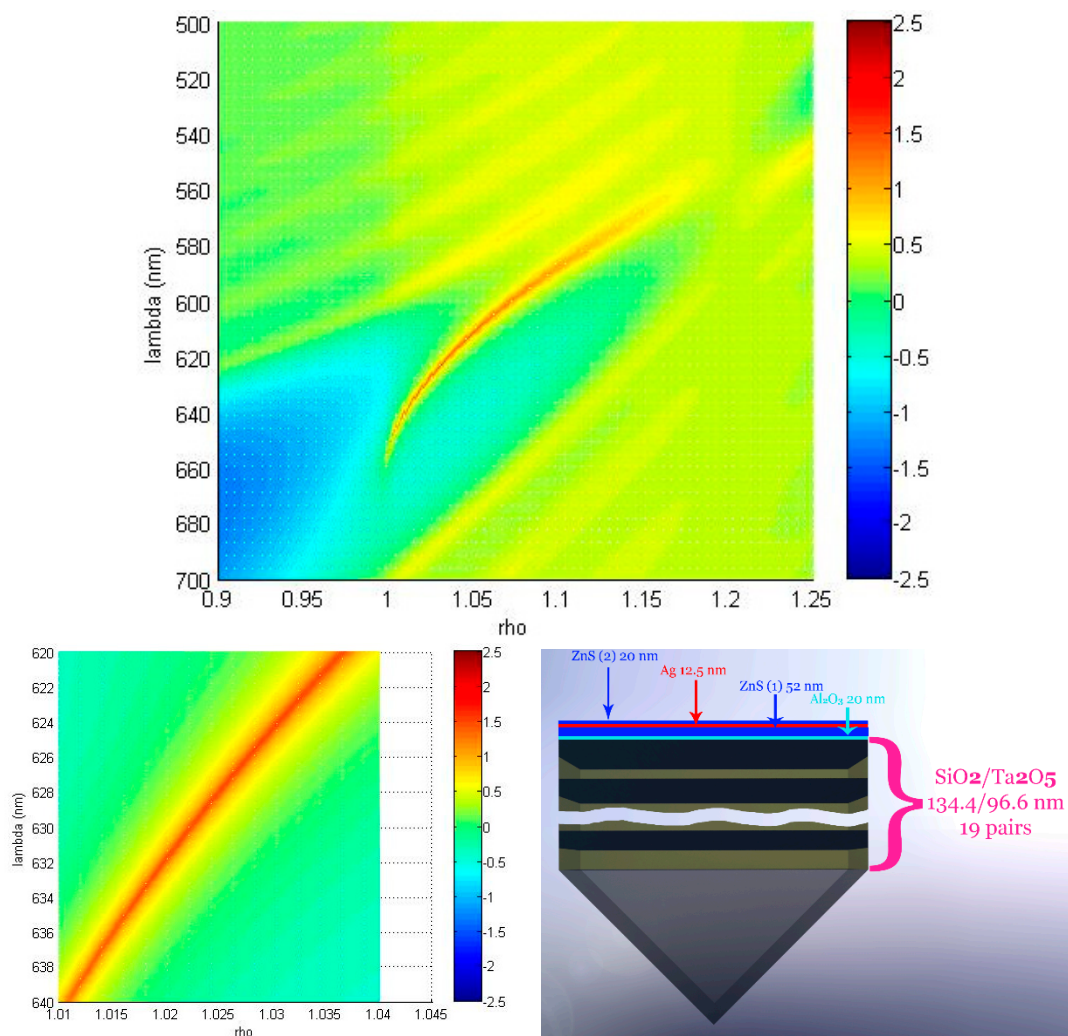


Figure 1. The calculated dispersion of the 1D Photonic Crystal (PC)-based structure (shown out of the scale in the lower right corner), supporting long-range surface plasmon polaritons (LRSPP) propagation along silver/ZnS/air interface. Color scale presents a value of $\log_{10}(I_e/I_0)$ where I_e, I_0 are respectively the intensities of light at the interface and at the entrance of the structure. In lower left corner, the magnified small part of the dispersion curve corresponding to the wavelength used is shown. See [27] for further details.

An essential difference of the structure at hand in comparison with the earlier used PC supporting LRSPP propagation [8–11,13] is the appearance of one additional protective ZnS(2) layer which necessitates the following modifications. In impedance representation [27], the condition for the

surface wave propagation remains the same: $Z_{left} + Z_{right} = 0$, where Z_{left} is an impedance of the system $\text{SiO}_2/(\text{HL})^{19}/\text{Al}_2\text{O}_3/\text{ZnS}(1)/\text{Ag}$ calculated using recursion formulae of Ref. [27] together with the formula (13) describing impedance of the photonic crystal there (for current purposes we can consider this PC as an infinite one). However, now Z_{right} is *not an* impedance of the infinite external media (air) equal to

$$Z_{air} = \sqrt{1 - (\rho/n_{air})}/n_{air} \quad (1)$$

but instead an impedance of the system $\text{ZnS}(2)/\text{air}$ which is equal to

$$Z_{right} = Z_{air} \frac{Z_{ZnS} - iZ_{air} \tan \alpha_{ZnS2}}{Z_{air} - iZ_{ZnS} \tan \alpha_{ZnS2}} \quad (2)$$

where $Z_{ZnS} = \sqrt{1 - (\rho/n_{ZnS})}/n_{ZnS}$, $\alpha_{ZnS2} = \frac{2\pi}{\lambda} n_{ZnS} d_{ZnS2} \sqrt{1 - (\rho/n_{ZnS})^2}$, and ρ is a “propagation parameter”, viz., an angular variable equal to $\rho = n_i \sin \theta_i$. This variable, according to the Snell’s law, remains the same for each layer having the refraction index n_i with θ_i being an angle between the propagating light and the normal to all interfaces [27]. This change is not negligible and must be taken into account because already for 20 nm-thick ZnS layer with the refraction index $n_{ZnS} = 2.318$ and $\rho = 1.017$ we have comparable values of $\alpha_{ZnS2} = 0.41$, $Z_{air} = 0.1285i$ and $Z_{ZnS} = 0.39$. At the same time, for many practical purposes, the whole effect of this additional layer can be seen simply as a relatively slight modification of the refraction index of an infinite external medium. Comparing (1) and (2) we see that for $\rho = 1.017$ Equation (1) gives the same impedance as Equation (2) if one put $n_{air} = n_{eff} = 1.03$ into Equation (1).

The results of our calculations are presented in Figure 1. It is easy to see that for He-Ne laser wavelength of 632.8 nm we do have a LRSPP wave characterized by the angular variable (propagation parameter) $\rho \cong 1.02$ and possessing quite strong thirty-fold enhancement of the intensity of light.

3. Experimental Results and Discussion

Schematic of an experimental setup together with the data attesting an observation of very narrow angular plasmon resonance in the light reflection from the aforementioned PC + Ag layer structure are presented in Figure 2. For the measurements of LRSPP, standard Kretschmann configuration employing quartz 45° prism on which the structure at question has been “glued” via a droplet of phase matching oil has been used [28]. Standard p-polarized He-Ne laser light (beam diameter around 5 mm) has been focused on the structure studied with 10 cm focal length lens, and the angular structure of the reflected light has been recorded observing the light spots at distances of 162 and/or 405 cm (both recordings of the light intensity with CMOS (complementary metal-oxide semiconductor) camera and processing of color digital photographs of the corresponding light spots were used leading to essentially the same results).

Surface plasmon excitation has been observed for conditions quite close to the normal incidence of the incoming light beam onto the prism entrance face: the corresponding angle was equal to 0.3° which results in the incidence angle onto the prism hypotenuse $\theta = 44.8^\circ$ giving the propagation parameter $\rho = 1.04$. Deviation of this value from the theoretical one is due to the deviations of actual refraction indices and layer thicknesses from the (theoretical or “searched for”) values used in calculations, and this is quite common for the field.

Another indication of the narrowness of the plasmon resonance in our structure has been obtained when we, in the same configuration, used unfocused He-Ne laser beam: for an optimal adjustment, the intensity of reflected light dropped from 5.9 mW (out of resonance) to 2.6 mW (in resonance) thus attesting that more than one half of an incoming radiation power has been transferred into the surface wave. The same experiment also was used to demonstrate the polarization dependence of the observed reflection minimum: the difference in the intensity of light reflected for out-of- and in-resonance conditions well followed the content of the p-polarized light in the incoming laser beam (it

was changed by the rotation of He-Ne laser having the polarization ratio not smaller than 50:1 without a polarizer), and such a difference was completely undetectable for the pure *s*-polarization case.

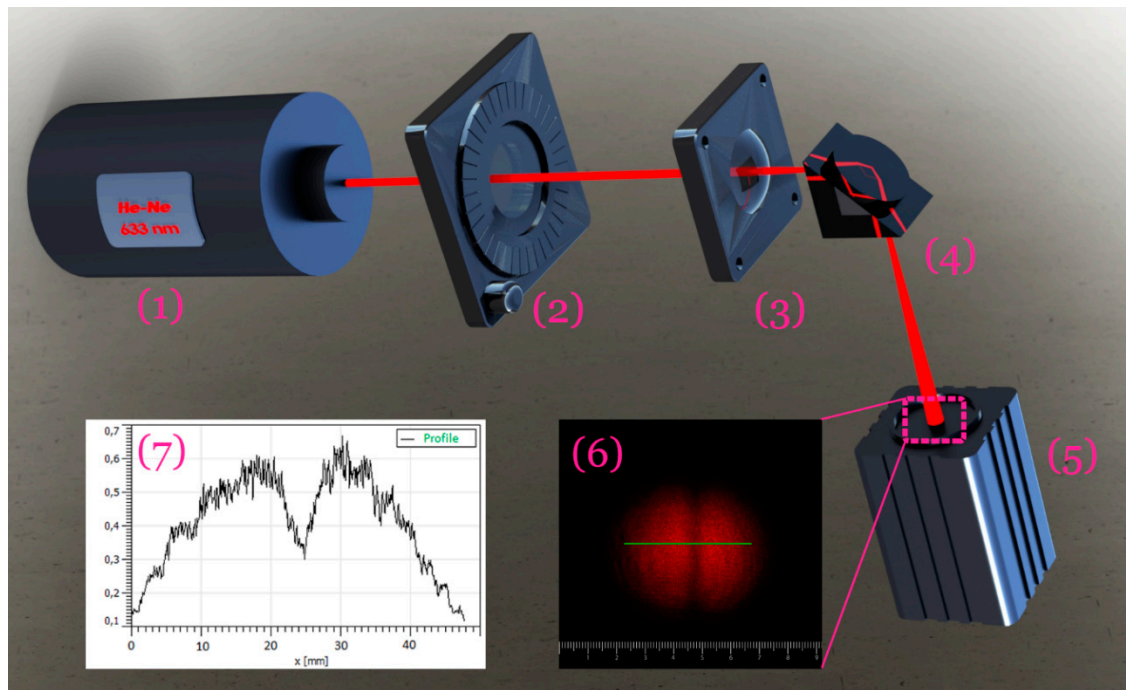


Figure 2. Schematic of an experimental equipment (1–5), color photograph of the reflected light spot (6) and intensity profile (7) measured at a distance of 405 cm. 1- He-Ne laser, 2-polarizer, 3-lens, 4-investigating structure $\text{SiO}_2/(\text{HL})^{19}/\text{Al}_2\text{O}_3/\text{ZnS}(1)/\text{Ag}/\text{ZnS}(2)/\text{air}$ glued to silica prism via a droplet of phase-matching oil, 5-CMOS (complementary metal-oxide semiconductor) camera.

The width of the angular resonance curve in Figure 2 is equal to ca. $\Delta\theta_{\text{air}} = 8 \cdot 10^{-4} \text{ rad}$ which corresponds to the surface plasmon propagation length l of approximately 180 microns. (Standard formula $l = \frac{\lambda}{2\pi\Delta\theta_{\text{pr}}n_{\text{pr}}\cos\theta_{\text{pr}}}$ was used. Here, the subscript *pr* corresponds to the values inside the prism; the value of $\Delta\theta_{\text{pr}}$ can be recalculated from the experimentally measured $\Delta\theta_{\text{air}}$ by applying Snell's law. For our case of almost normal incidence of light onto the prism catet $\Delta\theta_{\text{air}} \simeq n_{\text{pr}}\Delta\theta_{\text{pr}}$). Comparable, but slightly worse results with the angular width somewhat exceeding 10^{-3} rad were obtained when using a semiconductor cw fiber Bragg grating laser diode at the wavelength of 636.7 nm (QPhotonics LLC, Ann Arbor, MI, USA). This is the main result of our research, and it unambiguously attests the first realization of LRSPP for PC-supported silver nanofilms. The long-term stability of the prepared structures was noticed: the reflection parameters remained virtually the same during nine months of observations; the sample has been kept in usual room conditions in a polyethylene packet (not hermetically sealed).

The experimentally observed value $\rho = 1.04$ enables to determine the actual distribution of the square (EE^*) of electric field of SPP both inside an external medium (air, for which we take the refraction index equal to unity) and PC. For the former, we have an exponential decrease with the characteristic length $l_{\text{ext}} = \frac{\lambda}{4\pi\sqrt{\rho^2-1}} \cong 180 \text{ nm}$, that is much larger than the thickness of the ZnS layer adjacent to the silver nanofilm. Inside the Photonic Crystal, we have a standing wave with an exponentially decreasing envelope e^{Kz} . The value of K can be found applying e.g., Formulae (2) of [8]. An easy calculation gives $e^{K\Lambda} = 1.163$ which corresponds, for the PC period $\Lambda = 231 \text{ nm}$, to the characteristic decay length of $l_{\text{PC}} \cong 1.53 \mu\text{m}$. (Actually, the same value can be obtained calculating the transmission coefficient for one period of PC, see Section 2.4 of [27]). The precise field distribution inside a metal layer and, correspondingly, inside the dielectric layers immediately adjacent to it, is

quite sensitive to the exact thickness of metal layer and its refraction index which define the location of the minimum of an electric field inside the nanofilm, see a detailed discussion in [8,27]. This question is not relevant for the present work and has not been specially studied.

Discussing the obtained results, we first want to note that the observed LRSP propagation length in our silver nanofilm-based structures is quite comparable to the value of 160 microns reported in [8] for LRSP supported by a specially designed PC and ca. 5 nm—thick gold film at the wavelength of 710 nm. This is not surprising given the quite comparable “plasmonic qualities” of gold and silver at the (different) wavelengths at question: according to Palik’s book [29], at 710 nm we have $\epsilon_{Au} = -15.723 + 1.3413i$ which gives $\text{Im}(\sqrt{\frac{\epsilon_{Au}}{\epsilon_{Au}+1}}) = 0.0030i$ for the quantity describing the dissipation for SPP propagating along the interface air—infinately thick gold layer [28]. For our case, using the experimentally measured (by our group) value of the silver refraction index for a given wavelength, $n_{Ag} = 0.1345 + 3.986i$, that is $\epsilon_{Ag} = -15.8701 + 1.0722i$, we have $\text{Im}(\sqrt{\frac{\epsilon_{Ag}}{\epsilon_{Ag}+1}}) = 0.0023i$. However, one should also note more than two times smaller value of the metal layer thickness, ca. 5 nm, in experiments reported in [8]: a very important factor, given the inverse quadratic dependence of the LRSP dissipation on this same thickness [1–3]. All this, again, should be considered as the demonstration of truly high-quality silver nanofilm in our case.

Indeed, comparable LRSP propagation lengths have been observed also in experiments with Pd [10] and Co [12] nanofilms deposited onto the properly designed PC. The common characteristic feature here is that in all of these cases, the experimentally measured values, although are impressively large enough and much exceed the propagation lengths for simple metal—dielectric interfaces, turn out to be substantially smaller than those which could be achieved according to the theoretical predictions.

The latter can be estimated approximating the real system by a “symmetrical sandwich structure composed by an infinite medium with the refraction index n_{eff} —thin, with the thickness d_m , metal layer with the refraction index n_m —an infinite medium with the refraction index n_{eff}'' ”, using the value $n_{eff} = 1.03$ described above (varying of this value contributes to the result quite slightly). In the so called Leontovich approximation, see formula A3 from Konopsky paper [27] and other details therein, we have:

$$\frac{1}{\lambda} = \frac{1}{2\pi d_m n_m} \arctan \frac{2n_m n_{eff}^2 (\rho^2 - n_{eff}^2)^{1/2}}{n_{eff}^4 + n_m^2 n_{eff}^2 - n_m^2 \rho^2} \quad (3)$$

As a function of ρ , this is simple biquadratic equation

$$Q^2 n_m^4 \rho^4 - 2\rho^2 (Q^2 n_m^2 (n_{eff}^4 + n_m^2 n_{eff}^2) + 2n_m^2 n_{eff}^4) + Q^2 (n_{eff}^4 + n_m^2 n_{eff}^2)^2 + 4n_m^2 n_{eff}^6 = 0 \quad (4)$$

where $Q^2 = \tan^2 \frac{2\pi d_m n_m}{\lambda}$, and its solution gives us $\rho = 1.0033 + 6 \cdot 10^{-6}i$ corresponding to the theoretical propagation length of $\cong \frac{\lambda}{2\pi \text{Im}\rho} = 17$ mm, which is two orders of magnitude larger than the experimentally measured value. Similarly, for gold at 710 nm and for the thickness of 5 nm, cf. [8], we have $\text{Im}\rho \cong 10^{-6}$, for palladium at 739 nm with $d = 8$ nm and $n_{Pd} = 1.9 + 4.8i$ [10,27] we have $\text{Im}\rho \cong 10^{-5}$, and so forth.

Certainly, for the case of nanofilms, additional damping mechanisms exist and should be taken into account. The most well-known and fundamental one is the collision-induced scattering of conducting electrons at the walls of the nanofilm (“anomalous skin- and size-effects”) which has been profoundly discussed starting from the end of the forties (see e.g., [30,31] and references therein; see also [27]). For our purposes, it is sufficient to present here only the final formula pertinent for the imaginary part of the dielectric constant for a continuous thin film at a frequency ω [30]:

$$\epsilon'' = \epsilon''_{bulk} + \frac{3\omega_p^3}{8\omega^3} \frac{v_F}{c} \frac{1 + \cosh^2(\omega_p d/c)}{\sinh(\omega_p d/c) \cosh(\omega_p d/c) + \omega_p d/c} (1 - p) \quad (5)$$

where d is nanofilm thickness, ω_p is plasma frequency, v_F —Fermi velocity and p —the so called “scattering parameter” defined as a fraction of electrons specularly reflected on the walls. (Real part of the dielectric constant is practically non-affected by this same scattering). For a completely diffuse scattering, $p = 0$, Formula (5) gives the following limit for small thicknesses:

$$\varepsilon'' \cong \varepsilon''_{bulk} + \frac{3\omega_p^3 v_F}{8\omega^3 d} \quad (6)$$

Taking for estimations for our case of silver nanofilm $v_F = 1.4 \cdot 10^6$ m/s [32], $\hbar\omega_p = 9$ eV [33], $d = 12.5$ nm and the frequency corresponding to the He-Ne laser used, we have $\frac{3\omega_p^3 v_F}{8\omega^3 d} \cong 0.4$. This is non-negligible but still not such a significant change given that $\varepsilon''_{bulk} = n_{Ag}^2 = -15.87 + 1.07i$, and it results in the new value of an effective refractive index of the “gold in the nanofilm” $n_{film} = \sqrt{\varepsilon''} = 0.1846 + 3.99i$. Substitution of this value into formula (4) instead of $n_{Ag} = 0.1345 + 3.986i$ leads only to a minor change in the dissipation giving $\text{Im}\rho \cong 8 \cdot 10^{-6}$. The same conclusion can be drawn applying formula (6) for other cases, such as gold and palladium.

This same aforementioned noticeable difference between the experimentally observed and theoretically possible propagation lengths of LRSPP supported by Photonic Crystals should not be considered as surprising, because the ideal matching of the design of the PC and a real structure parameters, as well as ideal quality of all interfaces and materials, are needed (not to mention that in reality we certainly have a finite PC only). In any case, obtained values are already quite impressive and suitable for practical applications. Nevertheless, we should bear in mind that apparently there is still significant room for improvements in this field.

4. Conclusions

In the present paper, we report on the first experimental realization of Photonic Crystal—supported Long Range Surface Plasmon-Polaritons in thin, 12.5 nm-thick, silver nanofilms. These nanofilms have been deposited onto specially prepared and purpose—optimized for the task 1D Photonic Crystal, the design of which included as the most external part a thin ZnS layer earlier proposed as one of the most suitable adjacent layer to make a high-quality silver nanofilm. Another thin ZnS layer has been deposited over this Ag nanofilm, it is in contact with the atmosphere and serves as an indispensable external protective layer. The design of the PC takes into account the necessity of adding this layer, and the structure parameters have been optimized to enable the propagation of surface electromagnetic waves along the combined “thin layer of ZnS + air” external media—silver interface. Reasonable long-term stability of the structure has been observed.

The ultranarrow surface plasmon resonance corresponding to the LRSPP propagation length of 180 microns has been recorded. This value is quite large, and enables the practical use of similar structures as sensors, cf. [9–13], and the corresponding possibilities will be considered in the course of subsequent work.

Acknowledgments: This research has been supported by the Electron Science Research Institute, Edith Cowan University, WA, Australia, and by the grant N 200020-149424 of Swiss National Science Foundation. We thank the anonymous referee for referral to Ref. [23].

Author Contributions: S.K.S., M.V., G.D. and K.A. conceived and designed the research; M.V., M.N.E.A. and K.A. designed the silver nanofilm deposition conditions; S.K.S. designed the photon crystal, M.N.E.A. prepared the photon crystal, A.S. performed the optical studies of plasmons; all authors contributed to the writing of the paper and discussion.

Conflicts of Interest: The authors declare no conflict of interest.

References

1. Sarid, D. Long-range surface-plasma waves on very thin metal films. *Phys. Rev. Lett.* **1981**, *47*, 1927–1930. [CrossRef]

2. Craig, A.E.; Olson, G.A.; Sarid, D. Experimental observation of the long-range surface-plasmon polariton. *Opt. Lett.* **1983**, *8*, 380–382. [[CrossRef](#)] [[PubMed](#)]
3. Burke, J.J.; Stegeman, G.I.; Tamir, T. Surface-polariton-like waves guided by thin, lossy metal films. *Phys. Rev.* **1986**, *B33*, 5186–5201. [[CrossRef](#)]
4. Homola, J. Surface plasmon resonance sensors for detection of chemical and biological species. *Chem. Rev.* **2008**, *108*, 462–493. [[CrossRef](#)] [[PubMed](#)]
5. Piliarik, M.; Homola, J. Surface plasmon resonance (SPR) sensors: Approaching their limits? *Opt. Express* **2009**, *17*, 16505–16517. [[CrossRef](#)] [[PubMed](#)]
6. Krupin, O.; Asiri, H.; Wang, C.; Tait, R.N.; Berini, P. Biosensing using straight long-range surface plasmon waveguides. *Opt. Express* **2013**, *21*, 698–709. [[CrossRef](#)] [[PubMed](#)]
7. Berini, P. Long-range surface plasmon polaritons. *Adv. Opt. Phot.* **2009**, *1*, 484–588. [[CrossRef](#)]
8. Konopsky, V.N.; Alieva, E.V. Long-range propagation of plasmon polaritons in a thin metal film on a one-dimensional photonic crystal surface. *Phys. Rev. Lett.* **2006**, *97*, 253904. [[CrossRef](#)] [[PubMed](#)]
9. Konopsky, V.N.; Basmanov, D.V.; Alieva, E.V.; Sekatskii, S.K.; Dietler, G. Size-dependent hydrogen uptake behavior of Pd nanoparticles revealed by Photonic Crystal Surface Waves. *Appl. Phys. Lett.* **2012**, *100*, 0831108. [[CrossRef](#)]
10. Konopsky, V.N.; Basmanov, D.V.; Alieva, E.A.; Dolgy, D.I.; Olshansky, E.D.; Sekatskii, S.K.; Dietler, G. Registration of long-range surface plasmon resonance by angle-scattering feedback and its implementation for optical hydrogen sensing. *New J. Phys.* **2009**, *11*, 063049. [[CrossRef](#)]
11. Hamidi, S.M.; Ramezani, R.; Bananej, A. Hydrogen gas sensor based on long-range surface plasmons in lossy palladium film placed on photonic crystal stack. *Opt. Mater.* **2016**, *53*, 201–208. [[CrossRef](#)]
12. Ignatyeva, D.O.; Knyazev, G.A.; Kapralov, P.O.; Dietler, G.; Sekatskii, S.K.; Belotelov, V.I. Magneto-optical plasmonic heterostructure with ultranarrow resonance for sensing applications. *Sci. Rep.* **2016**, *6*, 28077. [[CrossRef](#)] [[PubMed](#)]
13. Alieva, E.V.; Konopsky, V.N.; Basmanov, D.V.; Sekatskii, S.K.; Dietler, G. Blue surface plasmon propagation along thin gold film—Gas interface and its use for sensitive nitrogen dioxide detection. *Opt. Commun.* **2013**, *309*, 148–152. [[CrossRef](#)]
14. Robertson, W.M.; May, M.S. Surface electromagnetic wave excitation on one-dimensional photonic band-gap arrays. *Appl. Phys. Lett.* **1999**, *74*, 1800. [[CrossRef](#)]
15. Konopsky, V.N.; Alieva, E.V. Photonic crystal surface waves for optical biosensors. *Anal. Chem.* **2007**, *79*, 4729–4735. [[CrossRef](#)] [[PubMed](#)]
16. Konopsky, V.N.; Karakouz, T.; Alieva, E.V.; Vicario, C.; Sekatskii, S.K.; Dietler, G. Photonic Crystal Biosensor based on Optical Surface Waves. *Sensors* **2013**, *13*, 2566–2578. [[CrossRef](#)] [[PubMed](#)]
17. Rostova, E.; Ben Adiba, C.; Dietler, G.; Sekatskii, S.K. Label-free optical biosensor based on photonic crystal reveals binding kinetics of antibodies to living bacterial cells *E. coli*. *Biosensors* **2016**, *6*, 52–57. [[CrossRef](#)] [[PubMed](#)]
18. Frascella, F.; Riccardi, S.; Rivoto, P.; Moi, V.; Giorgis, F.; Descrovi, E.; Michelotti, F.; Munzert, P.; Danz, N.; Napione, L. A Fluorescent One-Dimensional Photonic Crystal for Label-Free Biosensing Based on Bloch Surface Waves. *Sensors* **2013**, *13*, 2011–2022. [[CrossRef](#)] [[PubMed](#)]
19. Angelini, A.; Barakat, E.; Munzert, P.; Boarino, L.; De Leo, N.; Enrico, E.; Giorgis, F.; Herzig, H.P.; Pirri, C.F.; Descrovi, E. Focusing and Extraction of Light mediated by Bloch Surface Waves. *Sci. Rep.* **2015**, *4*, 5428. [[CrossRef](#)] [[PubMed](#)]
20. Kovalevich, T.; Ndao, A.; Suarez, M.; Tumenas, S.; Balevicius, Z.; Ramanavicius, A.; Balevicuita, I.; Häyrynen, M.; Roussey, M.; Kuittinen, M.; et al. Tunable Bloch surface waves in anisotropic photonic crystals based on lithium niobate thin films. *Opt. Lett.* **2016**, *41*, 5616–5619. [[CrossRef](#)] [[PubMed](#)]
21. Kovalevich, T.; Kim, M.S.; Belharet, D.; Robert, L.; Herzig, H.P.; Grosjean, T.; Bernal, M.P. Experimental evidence of Bloch surface waves on photonic crystals with thin film LiNbO₃ as a top layer. *Photonics Res.* **2017**, *5*, 649–653. [[CrossRef](#)]
22. Dubey, R.; Vosoughi Lahijani, B.; Barakat, E.; Häyrynen, M.; Roussey, M.; Kuittinen, M.; Herzig, H.P. Near-field characterization of a Bloch-surface-wave-based 2D disk Resonator. *Opt. Lett.* **2016**, *41*, 4867–4870. [[CrossRef](#)] [[PubMed](#)]
23. Quail, J.C.; Rako, J.G.; Simon, H.J. Long-range surface-plasmon modes in silver and aluminium films. *Opt. Lett.* **1983**, *8*, 377–379. [[CrossRef](#)] [[PubMed](#)]

24. Berini, P.; Charbonneau, R.; Lahoud, N.; Mattiussi, G. Characterisation of long-range surface-plasmon-polariton waveguides. *J. App. Phys.* **2005**, *98*, 043109. [[CrossRef](#)]
25. El Mouedden, Y.; Alghamedi, R.; Nur E Alam, M.; Vasiliev, M.; Alameh, K. Thin film coatings for solar and thermal radiation control prepared by physical vapor deposition. In Proceedings of the 2012 9th International Conference on High Capacity Optical Networks and Enabling Technologies (HONET), Istanbul, Turkey, 12–14 December 2012. [[CrossRef](#)]
26. Vasiliev, M.; Alghamedi, R.; Nur-E-Alam, M.; Alameh, K. Photonic microstructures for energy-generating clear glass and net-zero energy buildings. *Sci. Rep.* **2016**, *6*, 31831. [[CrossRef](#)] [[PubMed](#)]
27. Konopsky, V.N. Plasmon-polariton waves in nanofilms on one-dimensional photonic crystal surfaces. *New J. Phys.* **2010**, *12*, 093006. [[CrossRef](#)]
28. Raether, H. *Surface Plasmons on Smooth and Rough Surfaces and on Gratings*; Springer-Verlag: Berlin, Germany, 1988.
29. Palik, E.D. *Handbook of Optical Constants of Solids*; Academic: New York, NY, USA, 1985.
30. Thèye, M.-L. Investigation of the optical properties of Au by means of thin semitransparent films. *Phys. Rev.* **1976**, *B2*, 3060–3078. [[CrossRef](#)]
31. Dingle, R.B. The anomalous skin effect and the reflectivity of metals I. *Physica* **1953**, *19*, 311–347. [[CrossRef](#)]
32. Ashcroft, N.W.; Mermin, N.D. *Solid State Physics*; Saunders College Publishing: Forth Worth, TX, USA, 1976.
33. Ordal, M.A.; Long, L.L.; Bell, R.J.; Bell, S.E.; Bell, R.R.; Alexander, R.W.; Ward, C.A. Optical properties of the metals Al, Co., Cu, Au, Fe, Pb, Ni, Pd, Pt, Ag, Ti, and W in the infrared and far infrared. *Appl. Opt.* **1983**, *22*, 1099–1119. [[CrossRef](#)] [[PubMed](#)]



© 2018 by the authors. Licensee MDPI, Basel, Switzerland. This article is an open access article distributed under the terms and conditions of the Creative Commons Attribution (CC BY) license (<http://creativecommons.org/licenses/by/4.0/>).